

1 **Large increase in CH<sub>4</sub> emission following conversion of coastal**  
2 **marsh to aquaculture ponds explained by gas transport pathways**

3 Ping Yang<sup>a,b</sup>, Derrick Y.F. Lai<sup>c</sup>, Hong Yang<sup>d,e</sup>, Yongxin Lin<sup>a,b</sup>, Chuan Tong<sup>a,b\*</sup>, Yan  
4 Hong<sup>b</sup>, Yalan Tian<sup>b</sup>, Chen Tang<sup>b</sup>, Kam W. Tang<sup>f\*</sup>

5 <sup>a</sup>*Key Laboratory of Humid Subtropical Eco-geographical Process of Ministry of Education, Fujian*  
6 *Normal University, Fuzhou 350007, P.R. China*

7 <sup>b</sup>*School of Geographical Sciences, Fujian Normal University, Fuzhou 350007, P.R. China*

8 <sup>c</sup>*Department of Geography and Resource Management, The Chinese University of Hong Kong, Hong*  
9 *Kong, China*

10 <sup>d</sup>*College of Environmental Science and Engineering, Fujian Normal University, Fuzhou 350007,*  
11 *P.R. China*

12 <sup>e</sup>*Department of Geography and Environmental Science, University of Reading, Reading, RG6 6AB,*  
13 *UK*

14 <sup>f</sup>*Department of Biosciences, Swansea University, Swansea SA2 8PP, U. K.*

15

16

17

18 **\*Correspondence to:**

19 tongch@fjnu.edu.cn (Chuan Tong); k.w.tang@swansea.ac.uk (Kam W. Tang)

20 **ABSTRACT**

21 Reclamation of coastal wetlands for aquaculture use has been shown to have opposite  
22 effects on sediment CH<sub>4</sub> production potential and CH<sub>4</sub> emission flux, but the underlying  
23 reason remained unclear. In this study, we compared sediment properties, CH<sub>4</sub>  
24 production potential, emission flux, and CH<sub>4</sub> transport pathways between a brackish  
25 marsh and the nearby reclaimed aquaculture ponds in the Min River Estuary in  
26 southeastern China. Despite that the sediment CH<sub>4</sub> production potential in the ponds  
27 was significantly lower than the marsh, CH<sub>4</sub> emission flux in the ponds ( $17.4 \pm 2.7$  mg  
28 m<sup>-2</sup> h<sup>-1</sup>) was 11.9 times higher than the marsh ( $1.3 \pm 0.2$  mg m<sup>-2</sup> h<sup>-1</sup>). Plant-mediated  
29 transport accounted for 75% of the total CH<sub>4</sub> emission in the marsh, whereas ebullition  
30 accounted for 95% of the total CH<sub>4</sub> emission in the ponds. CH<sub>4</sub> emission flux in both  
31 habitat types was highest in the summer. These results suggest that the increase in CH<sub>4</sub>  
32 emission following the conversion of brackish marsh to aquaculture ponds was not  
33 caused by increased sediment CH<sub>4</sub> production, but rather by eliminating rhizospheric  
34 oxidation and shifting the major transport pathway to ebullition, allowing sediment CH<sub>4</sub>  
35 to bypass oxidative loss. This study improves our understanding of the impacts of  
36 modification of coastal wetlands on greenhouse gas dynamics.

37 **Keywords:** Methane (CH<sub>4</sub>) production; CH<sub>4</sub> emission; Gas transport pathway; Coastal  
38 wetland; Aquaculture ponds

## 39 **1. Introduction**

40 Human activities since the industrial revolution have significantly increased  
41 greenhouse gas emissions that have drastically changed the global climate (IPCC, 2021).  
42 Among the different greenhouse gases (GHGs), methane (CH<sub>4</sub>) has a global warming  
43 potential (GWP) 45 times that of carbon dioxide (CO<sub>2</sub>) over a 100-year time horizon  
44 (Neubauer and Megonigal, 2015), and CH<sub>4</sub> contributes ~20% of the global radiative forcing  
45 (IPCC, 2013). The atmospheric concentration of CH<sub>4</sub> has risen to 1909 ppbv in 2022  
46 (NOAA, 2022), exceeding the preindustrial level by ~150%. To increase food production,  
47 natural landscape is increasingly converted to farmlands and aquaculture ponds, which  
48 changes the hydrology, nutrient cycles, soil properties and biodiversity on a large scale  
49 (Andretta et al., 2016; Gao et al., 2019; Lin et al., 2022), often with an increase in CH<sub>4</sub>  
50 emission (IPCC, 2019; Tan et al., 2020). Comparing CH<sub>4</sub> production and emission and their  
51 environmental drivers between natural and modified lands is a key to understanding and  
52 predicting the effects of farming activities on climate change.

53 Despite covering only 5–8 % of the global land area, natural wetlands contribute 20–  
54 30 % of the global terrestrial carbon sequestration (Lal, 2008; Mitsch et al., 2013) and  
55 therefore play a crucial role in mitigating global climate change (Kayranli et al., 2010; Lu  
56 et al., 2017; Nahlik and Fennessy, 2016). Coastal wetlands alone are estimated to sequester  
57 approximately 44.6 Tg C yr<sup>-1</sup> thanks to their high sedimentation rate (Chmura et al., 2003).  
58 However, large areas of coastal wetlands around the world have been lost or degraded in  
59 the past century due to land development and modification (Murray et al., 2019), which

60 may increase the release of terrestrial CO<sub>2</sub> and CH<sub>4</sub> to the atmosphere (Pendleton et al.,  
61 2012; Tan et al., 2020; Verhoeven and Setter, 2010), with potential dire consequences on  
62 the climate.

63 Coastal wetlands in mainland China cover about 5.79 M ha across its southern and  
64 eastern seaboard. In the recent decades, China has experienced among the worst coastal  
65 wetland degradation due to continuous population and economic growth, rapid urbanization  
66 and infrastructure development (Sun et al., 2015). A large area of its coastal wetlands has  
67 been converted for agroforestry uses since the 1950s (He et al., 2021; Wang et al., 2014)  
68 and the reclamation of wetlands into aquaculture ponds is also widespread along the coast  
69 (Ren et al., 2019; Duan et al., 2020). In vegetated wetlands, plant-mediated transport of  
70 sediment CH<sub>4</sub> can be a dominant pathway for CH<sub>4</sub> emission to air (Bhullar et al., 2013;  
71 Jeffrey et al., 2019). However, construction of earthen aquaculture ponds not only removes  
72 the wetland vegetation, but also changes the hydrology from free-flowing water to standing  
73 water, modifies the sediment physical properties and microbial communities, and alters  
74 nutrient and organic loading to the sediment, all potentially affect CH<sub>4</sub> production and  
75 emission (Tan et al., 2020).

76 The Shanyutan Wetland (26°00'36"–26°03'42" N, 119°34'12"–119°40'40" E) is the  
77 largest tidal wetland within the Min River estuary in southeastern China (Figure 1). About  
78 30% of its area has been converted into shrimp aquaculture ponds since 2011. A study has  
79 shown that CH<sub>4</sub> emission from the aquaculture ponds was much higher than the nearby  
80 vegetated wetland (Yang et al., 2017); yet, a follow-on study showed that the sediment CH<sub>4</sub>

81 production potential in the ponds was significantly lower than the vegetated wetland (Yang  
82 et al., 2022). To resolve this paradox, we hypothesized that conversion of vegetated wetland  
83 to aquaculture ponds changes the transport pathways of sediment CH<sub>4</sub>, leading to an overall  
84 higher emission flux in the aquaculture ponds.

85 To test our hypothesis, we compared CH<sub>4</sub> emission flux and the main transport  
86 pathways between the aquaculture ponds and nearby wetland over a 33-month period. We  
87 also collected monthly samples of sediment and porewater from both habitat types over a  
88 10-month period to measure sediment properties and CH<sub>4</sub> production potential. The results  
89 improve our understanding of how conversion of vegetated wetland to aquaculture ponds  
90 impacts the climate by changing sediment CH<sub>4</sub> production and transport mechanisms and  
91 subsequent emission to air.

## 92 **2. Materials and methods**

### 93 *2.1. Study area and sampling frequency*

94 The Shanyutan Wetland region is characterized by a subtropical humid monsoonal  
95 climate, with 1,390 mm annual mean precipitation, 19.6 °C air temperature and 77.0%  
96 relative humidity (Yang et al., 2020). A large area of the wetland has been cleared of  
97 vegetation (mainly *Cyperus malaccensis* and *Spartina alterniflora*) and reclaimed for  
98 shrimp (*Litopenaeus vannamei*) aquaculture over the past decade (Yang et al., 2020). A  
99 brackish *C. malaccensis* marsh stand and three nearby aquaculture ponds were selected for  
100 the study (Figure 1c).

101 To measure plant-mediated CH<sub>4</sub> emission in the marsh, two sets of 1 m × 1 m plots (in

102 triplicate; < 5 m distance between plots) were established. One set of the plots was used as  
103 shoot clipping treatment (SCT) where the aboveground vegetation was removed and  
104 petroleum jelly was used to seal the clipped end of the stems to prevent gas release (Tong  
105 et al., 2012). The plants in the other set were left intact as the unclipped control treatment  
106 (UCT) (Hu et al., 2016; Tong et al., 2012).

107 The selected shrimp aquaculture ponds were 1.0–3.0 ha in area with a mean water  
108 depth of ~1.5 m during the farming period. The ponds were filled with seawater drawn from  
109 the estuary. Shrimp farming started in May and ended in November, producing a single  
110 crop. The shrimp were fed commercial food pellets daily. Further details of the aquaculture  
111 pond system and farming practice can be found elsewhere (Yang et al., 2020).

112 CH<sub>4</sub> flux measurements were taken 1–2 times each month between April 2019 and  
113 December 2021. Sediment and porewater samples were collected once every month  
114 between April 2019 and January 2020. Sediment samples (top 15 cm; triplicate) were  
115 collected using a steel corer (internal diameter 5 cm). Sediment porewater (top 15 cm) in  
116 the brackish marsh was sampled by *in situ* dialysis (Strack and Waddington, 2008; Tong et  
117 al., 2018). Porewater within the pond sediment was extracted by centrifugation in the  
118 laboratory (Bodmer et al., 2020; Matos et al., 2016). All field samples were stored in an ice-  
119 packed cooler and transported back to the laboratory within 4–6 hr.

## 120 2.2. CH<sub>4</sub> emission flux measurements

121 Within the marsh stand, gas emission samples from the SCT and UCT plots were  
122 collected using a static chamber (Tong et al., 2012; Xiang et al., 2015). The static chamber

123 was made of transparent polyvinyl chloride (PVC), with a top chamber (35 cm length × 35  
124 cm width × 100 cm height) and a bottom collar (35 cm length × 35 cm width × 30 cm  
125 height). The bottom collar was inserted into the marsh sediment, leaving only 5 cm above  
126 the sediment surface. Gas samples from the aquaculture ponds were collected using a  
127 floating chamber (*FC*) as described in previous studies ([Natchimuthu et al., 2016](#); [Yang et](#)  
128 [al., 2020](#)). The *FC* was made from an inverted plastic basin (polyethylene/plexiglas®),  
129 covering an area of 0.1 m<sup>2</sup> and a volume of 5.2 L, and was fitted with Styrofoam on the  
130 sides for floatation.

131 On each sampling date, gas samples were taken from each chamber headspace with a  
132 syringe into 50 mL aluminum-foil gas sample bags (Dalian Delin Gas Packing Co., Ltd.,  
133 China) at 0, 15, 30 and 45 min intervals. Upon return to the laboratory, the CH<sub>4</sub>  
134 concentrations in the gas sample bags were measured on a Shimadzu GC-2010 gas  
135 chromatograph (Kyoto, Japan) with a flame ionization detector (FID). The CH<sub>4</sub> fluxes (mg  
136 m<sup>-2</sup> h<sup>-1</sup>) were calculated according to [Hirota et al. \(2004\)](#) and [Yuan et al. \(2021\)](#).

### 137 2.3. Determination of CH<sub>4</sub> transport pathways

138 Within the marsh stand, the CH<sub>4</sub> flux measured in the UCT plot was a combination of  
139 diffusive, ebullitive and plant-mediated CH<sub>4</sub> fluxes, whereas the CH<sub>4</sub> flux measured in the  
140 SCT plot represented the combination of diffusive and ebullitive CH<sub>4</sub> fluxes. Therefore,  
141 plant-mediated CH<sub>4</sub> flux was deduced from the difference in CH<sub>4</sub> flux between UCT and  
142 SCT plots ([Ding et al., 2005](#); [Hu et al., 2016](#)).

143 The CH<sub>4</sub> flux measured by the *FC* method ( $F_T$ ) in the aquaculture ponds represented

144 the combination of ebullitive flux ( $F_E$ ) and diffusive flux ( $F_D$ ) (Chuang et al., 2017; Wu et  
145 al., 2019). To separate the two components,  $F_D$  was independently determined from surface-  
146 water dissolved  $CH_4$  concentrations and wind-dependent gas exchange velocity ( $k$ )  
147 according to the thin boundary layer model (Cole and Caraco 1998; Musenze et al., 2014;  
148 Wanninkhof et al., 1992). To determine dissolved  $CH_4$  concentrations, triplicate bubble-free  
149 water samples were collected from each pond (at 20 cm depth) using pre-weighed serum  
150 glass bottles, and upon return to the laboratory, dissolved  $CH_4$  concentrations were  
151 measured using the headspace equilibration method on a gas chromatograph (GC-2010 with  
152 FID, Shimadzu, Kyoto, Japan) (Borges et al., 2018; Musenze et al., 2014; Yang et al., 2019a,  
153 2020). Diffusive flux ( $F_D$ ;  $mg\ m^{-2}\ h^{-1}$ ) across the water-air interface was calculated as:

$$154 \quad F_D = k_x \times (C_w - C_{eq}) \times M \times 1000 \quad (\text{Eq. 1})$$

155 Where  $k_x$  is the gas transfer coefficient ( $m\ h^{-1}$ ) calculated from wind speed (Cole and Caraco,  
156 1998),  $C_w$  is the dissolved  $CH_4$  concentration ( $\mu mol\ L^{-1}$ ),  $C_{eq}$  is the air-equilibrated  
157 dissolved  $CH_4$  concentration ( $\mu mol\ L^{-1}$ ) in surface water for the *in situ* temperature and  
158 salinity,  $M$  is the molar mass of  $CH_4$  ( $16\ g\ mol^{-1}$ ). Afterward, ebullitive flux ( $F_E$ ) was  
159 calculated as the difference between  $F_T$  and  $F_D$  (Chuang et al., 2017; Xiao et al., 2017).

#### 160 2.4. Measurement of sediment $CH_4$ production potential

161 Triplicate sediment samples (top 15 cm) collected from each site were used in  
162 anaerobic slurry incubation experiment to measure  $CH_4$  production potentials (Bodmer et  
163 al., 2020; Minick et al., 2021; Vizza et al., 2017). In the laboratory, ~30 g of each sediment  
164 sample and 30 mL of *in situ* water were added to a 200 mL glass incubation bottle. The



165 bottle was flushed with pure nitrogen gas ( $N_2$ ) for 5–8 min to create an anoxic condition  
166 (Song et al., 2021; Vizza et al., 2017; Zhou et al., 2022) and then sealed with a sterile butyl  
167 rubber stopper. Subsequently, the bottles were incubated for 15 days at *in situ* temperature  
168 (14–30 °C). On Days 1, 3, 5, 7, 9, 11, 13 and 15, a 5-mL headspace gas sample was taken  
169 with a syringe from each bottle and 5 mL pure  $N_2$  gas was added back to maintain the  
170 pressure.  $CH_4$  concentrations in the extracted gas samples were analyzed on a gas  
171 chromatograph (GC-2010 with FID, Shimadzu, Kyoto, Japan). Sediment  $CH_4$  production  
172 potential was calculated from the slope of linear regression between headspace  $CH_4$   
173 concentration and incubation time for each sample bottle (Liu et al., 2019; Wassmann et al.,  
174 1998).

### 175 2.5. Ancillary environmental variables

176 Meteorological parameters, including wind speed ( $W_s$ ), air temperature ( $T_A$ ) and air  
177 pressure ( $A_P$ ), were recorded by an automated meteorological station in the Shanyutan  
178 Wetland. Sediment temperature ( $T_s$ ) and water temperature ( $T_w$ ) were measured *in situ*  
179 using a portable instrument (IQ150, IQ Scientific Instruments, USA). Dissolved oxygen  
180 concentration (DO) in the aquaculture pond water was measured with a multiparameter  
181 probe (550A YSI sonde, USA) at a 20-cm water depth. Subsamples of the sediment were  
182 freeze-dried, homogenized and ground to a fine powder for analysis of physicochemical  
183 properties. Sediment was diluted with deionized water before measuring pH (Orion 868 pH  
184 meter, USA; sediment-to-water ratio 1:2.5 w/v) and salinity (Eutech Instruments-Salt6  
185 salinity meter, USA; sediment-to-water ratio 1:5 w/v). Sediment TC (total carbon) and TN

186 (total nitrogen) were measured on a combustion analyzer (Elementar Vario MAX CN,  
187 Germany). Porewater was analyzed for  $\text{NH}_4^+$ -N concentration (flow injection analyzer;  
188 Skalar Analytical SAN<sup>++</sup>, Netherlands) and  $\text{Cl}^-$  and  $\text{SO}_4^{2-}$  concentrations (Dionex 2100 ion  
189 chromatograph).

## 190 *2.6. Statistical analysis*

191 All data were checked for normality and homogeneity of variance. Significant  
192 differences in environmental variables,  $\text{CH}_4$  production potential and  $\text{CH}_4$  flux between  
193 habitat types were tested by analysis of variance (ANOVA) using the SPSS version 22.0  
194 (IBM, Armonk, NY, USA). Spearman correlation analysis was done to evaluate the  
195 relationships between  $\text{CH}_4$  flux (or  $\text{CH}_4$  production potential) and various environmental  
196 variables, using the corrplot and Hmisc packages in R software (Version 4.1.0). The  
197 weighted response ratios ( $\text{RR}_{++}$ ) were calculated to assess the responses of sediment  $\text{CH}_4$   
198 production potential and  $\text{CH}_4$  flux to habitat modification, following [Hedges et al. \(1999\)](#)  
199 and [Tan et al. \(2019\)](#). Redundancy analysis (RDA) was performed to assess which  
200 environmental variables best explained the temporal variations in  $\text{CH}_4$  flux (or  $\text{CH}_4$   
201 production potential), using CANOCO 5.0 for Windows (Microcomputer Power, Ithaca,  
202 USA). All results were presented as mean  $\pm$  1 standard error, unless otherwise stated. To  
203 ease comparison, data were grouped by seasons where appropriate.

## 204 **3. Results**

### 205 *3.1. Water and sediment properties*

206 The physicochemical properties of sediment and porewater in the marsh and

207 aquaculture ponds were shown in [Table S1](#). Overall, there were no appreciable differences  
208 in sediment pH and porewater  $\text{SO}_4^{2-}$  between the two habitat types, but  $T_s$ , salinity, TC, TN,  
209 and porewater  $\text{NH}_4^+\text{-N}$  and  $\text{Cl}^-$  were all significantly lower in aquaculture ponds than in the  
210 marsh. When comparing across seasons ([Table 1](#)), we observed generally higher  $T_s$ ,  $T_w$ , TC  
211 and TN in the summer/autumn, but higher  $\text{Cl}^-$ ,  $\text{SO}_4^{2-}$  and DO in the winter ([Table S1](#)).

### 212 3.2. Differences in $\text{CH}_4$ production and emission between habitat types

213 The sediment  $\text{CH}_4$  production potential in the marsh ( $45.21 \pm 12.73 \text{ ng g}^{-1} \text{ d}^{-1}$ ) was  
214 significantly higher ( $p < 0.01$ ; [Figure S1a](#)), by 124.5% on average, than in the ponds  
215 ( $20.14 \pm 5.59 \text{ ng g}^{-1} \text{ d}^{-1}$ ).  $\text{CH}_4$  emission flux in the SCT marsh plots averaged  $0.31 \pm 0.05 \text{ mg}$   
216  $\text{m}^{-2} \text{ h}^{-1}$  (ranged  $0.03\text{--}1.29 \text{ mg m}^{-2} \text{ h}^{-1}$ ), which was less than the UCT plots (mean  $1.34 \pm 0.24$   
217  $\text{mg m}^{-2} \text{ h}^{-1}$ ; range  $0.25\text{--}8.78 \text{ mg m}^{-2} \text{ h}^{-1}$ ). The mean  $\text{CH}_4$  emission flux in the ponds was  
218 more than 10-fold higher, at  $17.4 \pm 2.7 \text{ mg m}^{-2} \text{ h}^{-1}$  ( $F_{\text{df}=1} = 31.419$ ,  $p < 0.0001$ ; [Figure S1b](#)).

219  $\text{CH}_4$  emission flux showed strong seasonal differences in both habitat types ([Figure](#)  
220 [S2](#)). Overall,  $\text{CH}_4$  emission flux in the marsh was highest in the summer, followed by spring,  
221 autumn and winter ([Figure S2a](#)), whereas  $\text{CH}_4$  emission in the ponds followed the order of  
222 summer > autumn > spring > winter ([Figure S2b](#)).

### 223 3.3. Transport pathways for $\text{CH}_4$ emission

224 Total  $\text{CH}_4$  emission flux in the marsh varied between  $0.2 \pm 0.1$  and  $8.8 \pm 7.5 \text{ mg m}^{-2} \text{ h}^{-1}$   
225 across all sampling dates ([Figure 2](#)). Plant-mediated  $\text{CH}_4$  emission flux, derived from the  
226 difference between UCT plots and SCT plots, was  $0.1\text{--}8.1 \text{ mg m}^{-2} \text{ h}^{-1}$  (average  $1.1 \pm 0.2 \text{ mg}$   
227  $\text{m}^{-2} \text{ h}^{-1}$ ), which accounted for 21–96 % ([Figure 3a](#)), average 75%, of the total emission in

228 the marsh. The rest of the emission was likely a combination of diffusion and ebullition.

229 Total CH<sub>4</sub> emission flux in the aquaculture ponds ranged from 0.1±0.4 to 127.1±13.3  
230 mg m<sup>-2</sup> h<sup>-1</sup> over the study period (Figure 2). Ebullition was the dominant transport pathway,  
231 accounting for 0.1–126.9 mg m<sup>-2</sup> h<sup>-1</sup>, or 45.6–99.8 % (average 85%) of the CH<sub>4</sub> emission  
232 flux in the ponds (Figure 3b). The remaining emission flux came from diffusion.

### 233 3.4. Responses of CH<sub>4</sub> production and emission to habitat modification

234 The Weighted response ratios (RR<sub>++</sub>) of sediment CH<sub>4</sub> production potential ( $PP_{CH_4}$ )  
235 and CH<sub>4</sub> emission flux ( $F_{CH_4}$ ) are shown in Figure 4. Conversion of the marsh to aquaculture  
236 ponds decreased sediment CH<sub>4</sub> production potential significantly ( $p<0.05$ ) by 6.9% (Figure  
237 4a), but increased CH<sub>4</sub> emission flux by 52.4% (Figure 4b).

### 238 3.5. Relationships between CH<sub>4</sub> emission and environmental variables

239 Spearman correlation analysis showed that CH<sub>4</sub> emission flux was positively  
240 correlated with  $T_A$ ,  $T_S$  and TC in both habitats ( $p<0.01$  or  $p<0.001$ ), but negatively  
241 correlated with  $A_p$ , sediment salinity, porewater Cl<sup>-</sup> and SO<sub>4</sub><sup>2-</sup> concentrations ( $p<0.01$  or  
242  $p<0.001$ ) (Figure 5). Moreover, CH<sub>4</sub> emission flux in the ponds was positively correlated  
243 with  $T_W$  but negatively with DO ( $p<0.001$ ; Figure 5b). Sediment CH<sub>4</sub> production potential  
244 and CH<sub>4</sub> emission flux were positively correlated with each other in both habitats ( $p<0.001$ ).

245 Based on the result of RDA,  $T_S$ , NH<sub>4</sub><sup>+</sup>-N, SO<sub>4</sub><sup>2-</sup> and TC were the variables that best  
246 explained the variation in CH<sub>4</sub> emission flux in the marsh (Figure 6a), of which  $T_S$   
247 accounted for the highest percentage (38.9%), followed by NH<sub>4</sub><sup>+</sup>-N (21.3%), SO<sub>4</sub><sup>2-</sup> (13.6%)  
248 and TC (11.7%). The CH<sub>4</sub> emission flux the aquaculture ponds was mostly driven by TC,

249 which explained 63.8% of the variation, followed by  $\text{NH}_4^+\text{-N}$  (15%) and  $T_s$  (5.5%) (Figure  
250 6b).

## 251 4. Discussion

### 252 4.1. Land conversion effects on $\text{CH}_4$ dynamics

253  $\text{CH}_4$  is produced in the sediment by methanogenic archaea through the stepwise  
254 degradation of organic matter under anoxic condition (Segers, 1998; Villa et al., 2020).  
255 Once produced,  $\text{CH}_4$  can be exported from the sediment to the atmosphere via different  
256 pathways (Bastviken et al., 2004; Jeffrey et al., 2019; Villa et al., 2020). The presence of  
257 marsh plants may affect  $\text{CH}_4$  dynamics in several ways. Deposition of organic carbon by  
258 the plants may increase sediment methanogenesis. As plants use their vascular systems for  
259 gaseous exchange between tissues, the process brings  $\text{O}_2$  to the below-ground biomass but  
260 may also accelerate the transport and release of sediment  $\text{CH}_4$  to air (Sorrell and Boon,  
261 1994). The overall effect may depend on the plant species, leading to different degrees of  
262 increase or decrease in  $\text{CH}_4$  emission relative to bare sediment (Gurbir et al., 2013). The  
263 contributions of plant-mediated transport to total  $\text{CH}_4$  emission vary widely between  
264 different wetlands, ranging from 8% to 98% (Jeffrey et al., 2019; Knoblauch et al., 2015;  
265 Korrensalo et al., 2022; Morrissey and Livingston, 1992). In the present study, we found  
266 that the marsh plots with clipped above-ground vegetation ( $0.3 \pm 0.1 \text{ mg m}^{-2} \text{ h}^{-1}$ ) had lower  
267  $\text{CH}_4$  emission flux than the plots with intact vegetation ( $1.3 \pm 0.2 \text{ mg m}^{-2} \text{ h}^{-1}$ ), indicating that  
268 the presence of *C. malaccensis* increased  $\text{CH}_4$  emission relative to bare marsh sediment,  
269 and plant-mediated transport accounted for on average 75%, at times close to 100%, of the

270 CH<sub>4</sub> emission in the marsh (Figure 3a).

271 A notable observation in this study was that CH<sub>4</sub> emission flux in the aquaculture  
272 ponds on average was much higher than the marsh (Figure S1b), suggesting that conversion  
273 of marsh stand to aquaculture ponds would increase the areal output of CH<sub>4</sub> from the  
274 Shanyutan Wetland. These results are consistent with an earlier study (Yang et al. 2017) and  
275 are in line with a meta-analysis showing that CH<sub>4</sub> emission fluxes increased by 347%  
276 following the conversion of coastal wetlands to aquaculture ponds (Tan et al., 2020).  
277 However, CH<sub>4</sub> production potential independently measured by incubation experiment was  
278 actually lower in the aquaculture pond sediment than in the marsh sediment (Figure S1),  
279 confirming the observations in an earlier study and which could be attributed to the lower  
280 organic content, lower methanogen diversity and weaker interactions among the  
281 methanogens in the pond sediment (Yang et al., 2022). It should be noted that the CH<sub>4</sub>  
282 production was measured by anoxic incubation of slurry and therefore it reflected the  
283 potential capacity of CH<sub>4</sub> production, rather than actual in situ CH<sub>4</sub> production.  
284 Nevertheless, the paradoxical observations suggest that a higher CH<sub>4</sub> emission was not  
285 necessarily an indication of a higher capacity of the sediment to produce CH<sub>4</sub>; rather, other  
286 factors need to be taken into consideration that might affect the fate of CH<sub>4</sub> in the system.

287 Net CH<sub>4</sub> emission is determined by the balance between CH<sub>4</sub> production and CH<sub>4</sub>  
288 consumption (Schimel, 1995; Korrensalo et al., 2022; Yang et al., 2019a). Methanogenesis  
289 in the sediment is driven by organic carbon substrates and activity of methanogens under  
290 anoxic condition. CH<sub>4</sub> from the sediment may be consumed by methanotrophs in the

291 overlying oxic water before reaching the atmosphere (Bastviken et al., 2008). The vascular  
292 systems of the marsh plants that facilitate CH<sub>4</sub> transport can also bring atmospheric oxygen  
293 belowground (Blossfeld et al., 2011; Korrensalo et al., 2022; Turner et al., 2020), potentially  
294 increasing CH<sub>4</sub> oxidation around the roots (Laanbroek, 2010). Some studies have reported  
295 that rhizospheric oxidation removes most of the CH<sub>4</sub> produced in the sediment (e.g.,  
296 Calhoun and King, 1997; Popp et al., 2000; Fritz et al., 2011). In addition, river flow and  
297 periodic tidal flushing within the marsh would increase DO level in surface sediment (Well  
298 et al., 2018), thereby enhancing CH<sub>4</sub> oxidation and minimizing CH<sub>4</sub> accumulation within  
299 the sediment (Tan et al., 2020; Yamamoto et al., 2011). This altogether perhaps explains the  
300 low CH<sub>4</sub> emission flux in our marsh stand despite the higher sediment CH<sub>4</sub> production  
301 potential.

302 Marsh vegetation was removed to create the aquaculture ponds within the Shanyutan  
303 Wetland; therefore, plant-mediated CH<sub>4</sub> emission and rhizospheric oxidation were absent  
304 in the ponds. Instead, CH<sub>4</sub> diffusing out of the sediment could be consumed by CH<sub>4</sub>  
305 oxidation within the water column before reaching the air. Indeed, our results showed that  
306 CH<sub>4</sub> emission flux in the ponds was strongly and negatively correlated with dissolved  
307 oxygen concentration (Figures 5 and 6). On the other hand, the stagnant nature of the pond  
308 water may allow CH<sub>4</sub> to accumulate and form bubbles in the sediment, and subsequent  
309 ebullition would allow the CH<sub>4</sub> to bypass oxidation within the water column (Yuan et al.,  
310 2021). Earlier studies have shown that porewater CH<sub>4</sub> in the pond sediment accumulated to  
311 a much higher level (51.5 μM; Yang et al., 2019b) than the marsh sediment (17.1 μM; Tong

312 [et al., 2018](#)). Consequently, despite the lower sediment CH<sub>4</sub> production potential in the  
313 ponds (Figure S1a), the CH<sub>4</sub> emission flux was more than 10-fold higher than the marsh,  
314 with ebullition accounting for on average 85% of the total CH<sub>4</sub> emission (Figure 3b). This  
315 percentage is similar to observations in freshwater aquaculture ponds ([Yuan et al., 2021](#))  
316 and it falls within the range (50–95 % via ebullition) reported for organic-rich shallow  
317 aquatic systems ([Natchimuthu et al., 2014](#); [Wang et al., 2021a](#); [Wu et al., 2019](#); [Zhang et](#)  
318 [al., 2020](#)).

#### 319 *4.2. Environmental drivers of temporal variations in CH<sub>4</sub> emission*

320 Our results show that both the brackish marsh and the aquaculture ponds in the  
321 Shanyutan Wetland were atmospheric CH<sub>4</sub> sources with similar seasonal variabilities  
322 (Figure 2). Higher CH<sub>4</sub> emissions occurred in the summer and lower emissions in the winter  
323 in both habitats (Figure S2), which is consistent with observations in others coastal wetlands  
324 ([Jacotot et al., 2019](#); [Olsson et al., 2015](#); [Yang et al., 2021](#)) and aquatic systems ([Borges, et](#)  
325 [al., 2018](#); [Praetzel et al., 2021](#); [Sierra et al., 2017](#); [Wu et al., 2019](#)). Despite the similar  
326 seasonal patterns, we suggest that the underlying causes differed when considering the  
327 respective dominant transport pathway and environmental drivers in each habitat type.

328 In the marsh stand, sediment carbon content (TC) was only moderately important in  
329 driving CH<sub>4</sub> emission flux (explaining 11.7% of the variation) (Figure 6), suggesting that  
330 CH<sub>4</sub> emission flux in the marsh was weakly coupled to methanogenesis in the sediment.  
331 Rather, sediment temperature ( $T_s$ ) was the strongest factor driving CH<sub>4</sub> emission flux,  
332 explaining 39.8% of the variation. Given that plant-mediated transport was the dominant



333 CH<sub>4</sub> emission pathway in the marsh, higher  $T_s$  in the summer might increase  
334 evapotranspiration rate leading to higher CH<sub>4</sub> emission, as has been observed in other  
335 vegetated wetlands (MacDonald et al., 1998). However, plant-mediated emission was  
336 irrelevant in the aquaculture ponds. Instead, the rise and fall of CH<sub>4</sub> emission flux followed  
337 the farming cycle: the start of farming activity in the summer would have increased organic  
338 substrate availability (from feeds and animal wastes) in the sediment and driven up CH<sub>4</sub>  
339 emission. Indeed, RDA analysis showed that sediment carbon content (TC) was the  
340 overwhelming factor that determined CH<sub>4</sub> emission flux in the aquaculture ponds (63.8%).  
341 As the farming season came to an end in the winter, CH<sub>4</sub> emission decreased accordingly.

342 In the present study, CH<sub>4</sub> emissions from the marsh and ponds also exhibited  
343 substantial inter-annual variability, with the coefficients of variation of 58% and 39%,  
344 respectively. This may be attributed to the differences in salinity ( $F_{df=2}=452.362$ ,  $p<0.001$ )  
345 as a result of interannual variations in precipitation (1807 mm in 2019, 1516 mm in 2020  
346 and 1439 mm in 2021; the MRE weather station), which affected competition between  
347 sulfate reducing bacteria and methanogens (Chambers et al., 2013; Neubauer et al., 2013;  
348 Vizza et al., 2017). This was further confirmed by the significant and negative relationship  
349 between CH<sub>4</sub> flux and sediment salinity in both habitat types ( $p<0.01$ ; Table S2).

#### 350 4.3. Limitations and caveats

351 There are some limitations and caveats in this study. Firstly, sediment CH<sub>4</sub> production  
352 potential was measured by incubating slurry in anoxic condition, which may not reflect the  
353 actual CH<sub>4</sub> production rate where the sediment oxygen level varies. In situ measurements

354 using tracer technique, without the need for incubation, may give more accurate CH<sub>4</sub>  
355 production rates (Ashley et al., 2021; Wang et al., 2021b). The conversion of coastal  
356 wetland to aquaculture ponds can exert significant impacts on sediment physicochemical  
357 properties and various microorganisms, including methanotrophs (Gao et al., 2019).  
358 However, we did not investigate CH<sub>4</sub> oxidizers or oxidation rate in this study, a knowledge  
359 gap in a fuller understanding of CH<sub>4</sub> dynamics in the system. In the aquaculture ponds, the  
360 shrimp may increase the release of sediment CH<sub>4</sub> via bioturbation (Bezerra et al., 2020;  
361 Yuan et al., 2021), but the effect can be patchy and difficult to quantify with the floating  
362 chamber method. Lastly, land conversion is widespread along the coast of China and the  
363 Asian Pacific, but different wetlands can be dominated by different types of vegetation and  
364 likewise, different aquaculture systems have different farmed species and management  
365 practices (e.g., feed applications, aeration). Because of the highly variable species-specific  
366 effects of vegetation on sediment CH<sub>4</sub> dynamics (Bridgham et al., 2013; Laanbroek, 2010),  
367 a more detailed comparative study across regions and system types will improve our  
368 understanding of the climate impact of aquaculture-related landscape modification.

369

## 370 **5. Conclusions**

371 Overall, the conversion of marsh stand to aquaculture ponds in the Shanyutan Wetland  
372 changed not only the sediment capacity to produce CH<sub>4</sub>, but also the main CH<sub>4</sub> emission  
373 pathway. Despite the lower CH<sub>4</sub> production potential in the pond sediment, CH<sub>4</sub> emission  
374 flux was higher thanks to the effective transport pathway through ebullition. Plant-mediated

375 transport was the main pathway for CH<sub>4</sub> emission in the marsh, but rhizospheric oxidation  
376 by the rooted vegetation likely had resulted in the much lower CH<sub>4</sub> emission flux despite  
377 the higher sediment CH<sub>4</sub> production potential. Therefore, the overall effect of land  
378 conversion was to increase the areal CH<sub>4</sub> output to air, which raises concerns of the climate  
379 impact of the fast-growing small-hold aquaculture sector in China.

380

### 381 **Declaration of competing interest**

382 The authors declare that they have no known competing financial interests or personal  
383 relationships that could have appeared to influence the work reported in this paper.

### 384 **Acknowledgements**

385 This research was supported by the National Natural Science Foundation of China  
386 (NSFC) (Grant No. 41801070, and 41671088), the National Natural Science Foundation of  
387 Fujian Province (No. 2020J01136), and the Minjiang Scholar Programme.

### 388 **References**

- 389 Ashley, K., Davis, K.J., Martini, A., Vinson, D.S., Gerlach, R., Fields, M.W., McIntosh, J.,  
390 2021. Deuterium as a quantitative tracer of enhanced microbial methane production.  
391 Fuel 289, 119959. <https://doi.org/10.1016/j.fuel.2020.119959>
- 392 Andreetta, A., Huertas, A.D., Lotti, M., Cerise, S., 2016. Land use changes affecting soil  
393 organic carbon storage along a mangrove swamp rice chronosequence in the Cacheu  
394 and Oio regions (northern Guinea-Bissau). Agr. Ecosyst. Environ. 216, 314–321.  
395 <https://doi.org/10.1016/j.agee.2015.10.017>
- 396 Bastviken, D., Cole, J.J., Pace, M.L., Van de Bogert, M.C., 2008. Fates of methane from

397 different lake habitats: connecting whole-lake budgets and CH<sub>4</sub> emissions. J. Geophys.  
398 Res. 113, G02024. <https://doi.org/10.1029/2007JG000608>

399 Bridgham, S. D., Cadillo-Quiroz, H., Keller, J.K., Zhuang, Q., 2013. Methane emissions  
400 from wetlands: biogeochemical, microbial, and modeling perspectives from local to  
401 global scales. Global Change Biol. 19(5), 1325-1346.  
402 <https://doi.org/10.1111/gcb.12131>

403 Bezerra, M.P., McGinnis, D.F., Bezerra-Neto, J.F., Barbosa, F.A.R., 2020. Is it stochastic?  
404 *Chaoborus larvae* bioturbation likely affect the timing of daily methane (CH<sub>4</sub>)  
405 ebullitive flux in a tropical reservoir. Hydrobiologia 847, 3291–3308.  
406 <https://doi.org/10.1007/s10750-020-04331-w>

407 Bhullar, G.S., Edwards, P.J., Olde Venterink, H., 2013. Variation in the plant-mediated  
408 methane transport and its importance for methane emission from intact wetland peat  
409 mesocosms. J. Plant Ecol. 6(4), 298–304. <https://doi.org/10.1093/jpe/rts045>

410 Blossfeld, S., Gansert, D., Thiele, B., Kuhn, A.J., Löscher, R., 2011. The dynamics of oxygen  
411 concentration, pH value, and organic acids in the rhizosphere of *Juncus spp.* Soil Biol.  
412 Biochem. 43(6), 1186–1197. <https://doi.org/10.1016/j.soilbio.2011.02.007>

413 Bodmer, P., Wilkinson, J., Lorke, A., 2020. Sediment properties drive spatial variability of  
414 potential methane production and oxidation in small streams. J. Geophys. Res.-Biogeo.  
415 125(1), e2019JG005213. <https://doi.org/10.1029/2019JG005213>

416 Borges, A.V., Speeckaert, G., Champenois, W., Scranton, M.I., Gypens, N., 2018.  
417 Productivity and temperature as drivers of seasonal and spatial variations of dissolved  
418 methane in the Southern Bight of the North Sea. Ecosystems 21(4), 583–599.  
419 <https://doi.org/10.1007/s10021-017-0171-7>

420 Calhoun, A., King, G.M., 1997. Regulation of root-associated methanotrophy by oxygen  
421 availability in the rhizosphere of two aquatic macrophytes. Appl. Environ. Microb.  
422 63(8), 3051-3058. <https://doi.org/10.1089/oli.1.1997.7.439>

423 Chambers, L.G., Osborne, T.Z., Reddy, K.R., 2013. Effect of salinity-altering pulsing  
424 events on soil organic carbon loss along an intertidal wetlands gradient: a laboratory

425 experiment. *Biogeochemistry* 115, 363–383. [https://doi.org/10.1007/s10533-013-](https://doi.org/10.1007/s10533-013-9841-5)  
426 [9841-5](https://doi.org/10.1007/s10533-013-9841-5)

427 Chmura, G.L., Anisfeld, S.C., Cahoon, D.R., Lynch, J.C., 2003. Global carbon  
428 sequestration in tidal, saline wetland soils. *Global Biogeochem. Cy.* 17(4), 1111.  
429 <https://doi.org/10.1029/2002GB001917>

430 Chuang, P.-C., Young, M.B., Dale, A.W., Miller, L.G., Herrera-Silveira, J.A., Paytan, A.,  
431 2017. Methane fluxes from tropical coastal lagoons surrounded by mangroves, Yucatán,  
432 Mexico. *J. Geophys. Res. Biogeosci.*, 122(5), 1156-1174.  
433 <https://doi.org/10.1002/2017JG003761>

434 Cole, J.J., Caraco, N.F., 1998. Atmospheric exchange of carbon dioxide in a low-wind  
435 oligotrophic lake measured by the addition of SF<sub>6</sub>. *Limnol. Oceanogr.* 43(4), 647-656.  
436 <https://doi.org/10.4319/lo.1998.43.4.0647>

437 Ding, W.X., Cai, Z.C., Tsuruta, H., 2005. Plant species effects on methane emissions from  
438 freshwater marshes. *Atmos. Environ.* 39, 3199–3207.  
439 <https://doi.org/10.1016/j.atmosenv.2005.02.022>

440 Duan, Y.Q., Li, X., Zhang, L.P., Chen, D., Liu, S.A., Ji, H.Y., 2020. Mapping national-scale  
441 aquaculture ponds based on the Google Earth Engine in the Chinese coastal zone.  
442 *Aquaculture* 520, 734666. <https://doi.org/10.1016/j.aquaculture.2019.734666>

443 Fritz, C., Pancotto, V.A., Elzenga, J.T.M., Visser, E.J.W., Grootjans, A.P., Pol, A., Iturraspe,  
444 R., Roelofs, J.G.M., Smolders, A.J.P., 2011. Zero methane emission bogs: Extreme  
445 rhizosphere oxygenation by cushion plants in Patagonia. *New Phytol.* 190(2), 398–408.  
446 <https://doi.org/10.1111/j.1469-8137.2010.03604.x>

447 Gao, D.Z., Liu, M., Hou, L.J., Derrick, Y.F.L., Wang, W.Q., Li, X.F., Zeng, A.Y., Zheng,  
448 Y.L., Han, P., Yang, Y., Yin, G.Y., 2019. Effects of shrimp-aquaculture reclamation on  
449 sediment nitrate dissimilatory reduction processes in a coastal wetland of southeastern  
450 China. *Environ. Pollut.* 255, 113219. <https://doi.org/10.1016/j.envpol.2019.113219>

451 He, G.S., Wang, K.Y., Zhong, Q.C., Zhang, G.L., van den Bosch, C.K., Wang, J.T., 2021.  
452 Agroforestry reclamations decreased the CO<sub>2</sub> budget of a coastal wetland in the  
453 Yangtze estuary. *Agr. Forest Meteorol.* 296, 108212.

454 <https://doi.org/10.1016/j.agrformet.2020.108212>

455 Hedges, L.V., Gurevitch, J., Curtis, P.S., 1999. The meta-analysis of response ratios in  
456 experimental ecology. *Ecology* 80, 1150–1156. <https://doi.org/10.2307/177062>

457 Hirota, M., Tang, Y.H., Hu, Q.W., Hirata, S., Tomomichi, K., Mo, H.W., Cao, G.M., Mariko,  
458 S., 2004. Methane emissions from different vegetation zones in a Qinghai-Tibetan  
459 Plateau wetland. *Soil. Biol. Biochem.* 36, 737–748.  
460 <https://doi.org/10.1016/j.soilbio.2003.12.009>

461 Hu, Q.W., Cai, J.Y., Yao, B., Wu, Q., Wang, Y.Q., Xu, X.L., 2016. Plant-mediated methane  
462 and nitrous oxide fluxes from a carex meadow in Poyang Lake during drawdown  
463 periods. *Plant Soil* 400, 367–380. <http://dx.doi.org/10.1007/s11104-015-2733-9>

464 Jacotot, A., Marchand, C., Allenbach, M., 2019. Biofilm and temperature controls on  
465 greenhouse gas (CO<sub>2</sub> and CH<sub>4</sub>) emissions from a *Rhizophora* mangrove soil (New  
466 Caledonia). *Sci. Total Environ.* 650(Part 1), 1019–1028.  
467 <https://doi.org/10.1016/j.scitotenv.2018.09.093>

468 Jeffrey, L.C., Maher, D.T., Johnston, S.G., Kelaher, B.P., Steven, A., Tait, D.R., 2019.  
469 Wetland methane emissions dominated by plant-mediated fluxes: Contrasting  
470 emissions pathways and seasons within a shallow freshwater subtropical wetland.  
471 *Limnol. Oceanogr.* 64, 1895–1912. <https://doi.org/10.1002/lno.11158>

472 Kayranli, B., Scholz, M., Mustafa, A., & Hedmark, Å., 2010. Carbon storage and fluxes  
473 within freshwater wetlands: A critical review. *Wetlands* 30, 111–124.  
474 <https://doi.org/10.1007/s13157-009-0003-4>

475 Knoblauch, C., Spott, O., Evgrafova, S., Pfeiffer, E.M., 2015. Regulation of methane  
476 production, oxidation, and emission by vascular plants and bryophytes in ponds of the  
477 northeast Siberian polygonal tundra. *J. Geophys. Res.-Biogeosci.* 120, 2525–2541.  
478 <https://doi.org/10.1002/2015JG003053>

479 Korrensalo, A., Mammarella, I., Alekseychik, P., Vesala, T., Tuittila, E.-S., 2022. Plant  
480 mediated methane efflux from a boreal peatland complex. *Plant Soil* 471, 375–392.  
481 <https://doi.org/10.1007/s11104-021-05180-9>

- 482 IPCC, 2021. Summary for Policymakers. In: *Climate Change 2021: The Physical Science*  
483 *Basis. Contribution of Working Group I to the Sixth Assessment Report of the*  
484 *Intergovernmental Panel on Climate Change* [Masson-Delmotte, V., Zhai, P., Pirani,  
485 A., Connors, S.L., Péan, C., Berger, S., Caud, N., Chen, Y., Goldfarb, L., Gomis, M.I.,  
486 Huang, M., Leitzell, K., Lonnoy, E., Matthews, J.B.R., Maycock, T.K., Waterfield, T.,  
487 Yelekçi, O., Yu, R., Zhou B., (eds.)]. Cambridge University Press, In Press.
- 488 IPCC, 2013. In: Stocker, T.F., Qin, D., Plattner, G.K., Tignor, M., Allen, S.K., Boschung,  
489 J., Nauels, A., Xia, Y., Bex, V., Midgley, P.M. (Eds.), *Climate Change 2013: the*  
490 *Physical Science Basis. Contribution of Working Group I to the Fifth Assessment*  
491 *Report of the Intergovernmental Panel on Climate Change*. Cambridge University  
492 Press, Cambridge, United Kingdom and New York, NY, USA.
- 493 IPCC, 2019. In: Calvo Buendia, E., Tanabe, K., Kranjc, A., Baasansuren, J., Fukuda, M.,  
494 Ngarize, S. (Eds.), *2019 Refinement to the 2006 IPCC Guidelines for National*  
495 *Greenhouse Gas Inventories, Volum 4*. IPCC, Switzerland. Kanagawa, Japan.
- 496 Laanbroek, H.J., 2010. Methane emission from natural wetlands: interplay between  
497 emergent macrophytes and soil microbial processes. A mini-review. *Annals of Botany*,  
498 105(1), 141-153. <https://doi.org/10.1093/aob/mcp201>
- 499 Lal, R., 2008. Carbon sequestration. *Philos. Trans. R. Soc. B-Biol. Sci.* 363(1492), 815–  
500 830. <https://doi.org/10.1098/rstb.2007.2185>
- 501 Lin, Q.W., Wang, S.S., Li, Y.C., Riaz, L., Yu, F., Yang, Q.X., Han, S.J., Ma, J.M., 2022.  
502 Effects and mechanisms of land-types conversion on greenhouse gas emissions in the  
503 Yellow River floodplain wetland. *Sci. Total Environ.* 813, 152406.  
504 <http://dx.doi.org/10.1016/j.scitotenv.2021.152406>
- 505 Liu, J.G., Hartmann, S.C., Keppler, F., Lai, D.Y.F., 2019. Simultaneous abiotic production  
506 of greenhouse gases (CO<sub>2</sub>, CH<sub>4</sub>, and N<sub>2</sub>O) in Subtropical Soils. *J. Geophys. Res.-*  
507 *Biogeo.* 124. <https://doi.org/10.1029/2019JG005154>
- 508 Lu, W., Xiao, J., Liu, F., Zhang, Y., Liu, C., Lin, G., 2017. Contrasting ecosystem CO<sub>2</sub>  
509 fluxes of inland and coastal wetlands: A meta-analysis of eddy covariance data. *Glob.*  
510 *Change Biol.* 23, 1180–1198. <https://doi.org/10.1111/gcb.13424>

511 MacDonald, J.A., Fowler, D., Hargreaves, K.J., Skiba, U., Leith, I.D., Murray, M.B., 1998.  
512 Methane emission rates from a northern wetland; response to temperature, water table  
513 and transport. *Atmos. Environ.* 32(19), 3219–3227. [https://doi.org/10.1016/S1352-](https://doi.org/10.1016/S1352-2310(97)00464-0)  
514 [2310\(97\)00464-0](https://doi.org/10.1016/S1352-2310(97)00464-0)

515 Matos, C. R. L., Mendoza, U., Diaz, R., Moreira, M., Belem, A. L., Metzger, E.,  
516 Albuquerque, A.L.S., Machado, W., 2016. Nutrient regeneration susceptibility under  
517 contrasting sedimentary conditions from the Rio de Janeiro coast, Brazil. *Mar. Pollut.*  
518 *Bull.* 108, 297–302. <https://doi.org/10.1016/j.marpolbul.2016.04.046>

519 Minick, K.J., Mitra, B., Li, X.F., Fischer, M., Aguilos, M., Prajapati, P., Noormets, A., King,  
520 J.S., 2021. Wetland microtopography alters response of potential net CO<sub>2</sub> and  
521 CH<sub>4</sub> production to temperature and moisture: Evidence from a laboratory experiment.  
522 *Geoderma* 402, 115367. <https://doi.org/10.1016/j.geoderma.2021.115367>

523 Mitsch, W.J., Bernal, B., Nahlik, A.M., Mander, Ü., Zhang, L., Anderson, C.J., Jørgensen,  
524 S.E., Brix, H., 2013. Wetlands, carbon, and climate change. *Landsc. Ecol.* 28(4), 583–  
525 597. <https://doi.org/10.1007/s10980-012-9758-8>

526 Morrissey, L.A., Livingston, G.P., 1992. Methane emissions from Alaska Arctic tundra: an  
527 assessment of local spatial variability. *J. Geophys. Res.-Atmos.* 97, 16661–16670.  
528 <https://doi.org/10.1029/92JD00063>

529 Murray, N.J., Phinn, S.R., DeWitt, M., Ferrari, R., Johnston, R., Lyons, M.B., Clinton, N.,  
530 Thau, D., Fuller, R.A., 2019. The global distribution and trajectory of tidal flats. *Nature*,  
531 565, 222–225. <https://doi.org/10.1038/s41586-018-0805-8>

532 Musenze, R.S., Grinham, A., Werner, U., Gale, D., Sturm, K., Udy, J., Yuan, Z.G., 2014.  
533 Assessing the spatial and temporal variability of diffusive methane and nitrous oxide  
534 emissions from subtropical freshwater reservoirs. *Environ. Sci. Technol.* 48, 14499–  
535 14507. <https://doi.org/10.1021/es505324h>

536 Nahlik, A.M., Fennessy, M.S., 2016. Carbon storage in US wetlands. *Nat. Commun.* 7,  
537 13835. <https://doi.org/10.1038/ncomms13835>

538 Natchimuthu, S., Panneer Selvam, B., Bastviken, D., 2014. Influence of weather variables



539 on methane and carbon dioxide flux from a shallow pond. *Biogeochemistry* 119, 403–  
540 413. <https://doi.org/10.1007/s10533-014-9976-z>

541 Natchimuthu, S., Sundgren, I., Gålfalk, M., Klemedtsson, L., Crill, P., Danielsson, Å.,  
542 Bastviken, D., 2016. Spatio-temporal variability of lake CH<sub>4</sub> fluxes and its influence  
543 on annual whole lake emission estimates. *Limnol. Oceanogr.* 61(S1), S13–S26.  
544 <https://doi.org/10.1002/lno.10222>

545 NOAA(National Oceanic and Atmospheric Administration), 2022. Carbon cycle  
546 greenhouse gases: Trends in CH<sub>4</sub>. Available in:  
547 [https://www.esrl.noaa.gov/gmd/ccgg/trends\\_ch4/](https://www.esrl.noaa.gov/gmd/ccgg/trends_ch4/)

548 Neubauer, S.C., Franklin, R.B., Berrier, D.J., 2013. Saltwater intrusion into tidal freshwater  
549 marshes alters the biogeochemical processing of organic carbon. *Biogeosciences* 10,  
550 8171–8183. <https://doi.org/10.5194/bg-10-8171-2013>

551 Neubauer, S.C., Megonigal, J.P., 2015. Moving beyond global warming potentials to  
552 quantify the climatic role of ecosystems. *Ecosystems* 18, 1000–1013.  
553 <https://doi.org/10.1007/s10021-015-9879-4>

554 Olsson, L., Ye, S., Yu, X., Wei, M., Krauss, K.W., Brix, H., 2015. Factors influencing CO<sub>2</sub>  
555 and CH<sub>4</sub> emissions from coastal wetlands in the Liaohe Delta, Northeast China.  
556 *Biogeosciences* 12, 4965–4977. <https://doi.org/10.5194/bg-12-4965-2015>

557 Pendleton, L., Donato, D. C., Murray, B. C., Crooks, S., Jenkins, W. A., Sifleet, S., Craft,  
558 C., Fourqurean, J.W., Kauffman, J.B., Marbà, N., Megonigal, P., Pidgeon, E., Herr, D.,  
559 Gordon, D., Baldera, A., 2012. Estimating global “blue carbon” emissions from  
560 conversion and degradation of vegetated coastal ecosystems. *PLoS ONE*, 7, e43542.  
561 <https://doi.org/10.1371/journal.pone.0043542>

562 Popp, T.J., Chanton, J.P., Whiting, G.J., Grant, N., 2000. Evaluation of methane oxidation  
563 in the rhizosphere of a *Carex* dominated fen in northcentral Alberta, Canada.  
564 *Biogeochemistry* 51(3), 259–281. <https://doi.org/10.1023/A:1006452609284>

565 Praetzel, L.S.E., Schmiedeskamp, M., Knorr, K.H., 2021. Temperature and sediment  
566 properties drive spatiotemporal variability of methane ebullition in a small and shallow  
567 temperate lake. *Limnol. Oceanogr.* 66(7), 2598–2610.

568 <https://doi.org/10.1002/Ino.11775>

569 Ren, C.Y., Wang, Z.M., Zhang, Y.Z., Zhang, B., Chen, L., Xia, Y.B., Xiao, X.M., Doughty,  
570 R.B., Liu, M.Y., Jia, M., Mao, D.H., Song, K.S., 2019. Rapid expansion of coastal  
571 aquaculture ponds in China from Landsat observations during 1984–2016. *Int. J. Appl.*  
572 *Earth Obs.* 82, 101902. <https://doi.org/10.1016/j.jag.2019.101902>

573 Segers, R., 1998. Methane production and methane consumption: A review of processes  
574 underlying wetland methane fluxes. *Biogeochemistry* 41, 23–51.  
575 <https://doi.org/10.1023/A:1005929032764>

576 Sierra, A., Jiménez-López, D., Ortega, T., Ponce, R., Bellanco, M. J., Sánchez-Leal, R.,  
577 Forjaa, J., 2017. Spatial and seasonal variability of CH<sub>4</sub> in the eastern Gulf of Cadiz  
578 (SW Iberian Peninsula). *Sci. Total Environ.* 590-591, 695–707.  
579 <https://doi.org/10.1016/j.scitotenv.2017.03.030>

580 Song, Y.T., Chen, L.Y., Kang, L.Y., Yang, G.B., Qin, S.Q., Zhang, Q.W., Mao, C., Kou, D.,  
581 Fang, K., Feng, X.H., Yang, Y.H., 2021. Methanogenic community, CH<sub>4</sub> production  
582 potential and its determinants in the active layer and permafrost deposits on the Tibetan  
583 Plateau. *Environ. Sci. Technol.* 55, 11412-11423.  
584 <https://doi.org/10.1021/acs.est.0c07267>

585 Sorrell, B. K., Boon P. I., 1994. Convective gas flow in *Eleocharis sphacelata* R. Br.:  
586 Methane transport and release from wetlands. *Aquat. Bot.* 47, 197–212.  
587 [https://doi.org/10.1016/0304-3770\(94\)90053-1](https://doi.org/10.1016/0304-3770(94)90053-1)

588 Strack, M., Waddington, J.M., 2008. Spatiotemporal variability in peatland subsurface  
589 methane dynamics. *J. Geophys. Res.-Biogeo.* 113, G02010.  
590 <https://doi.org/10.1029/2007JG000472>

591 Sun, Z.G., Sun, W.G., Tong, C., Zeng, C.S., Yu, X., Mou, X.J., 2015. China's coastal  
592 wetlands: Conservation history, implementation efforts, existing issues and strategies  
593 for future improvement. *Environ. Int.* 79, 25–41.  
594 <http://dx.doi.org/10.1016/j.envint.2015.02.017>

595 Tan, L.S., Ge, Z.M., Zhou, X.H., Li, S.H, Li, X.Z., Tang, J.W., 2020. Conversion of coastal

596 wetlands, riparian wetlands, and peatlands increases greenhouse gas emissions: A  
597 global meta-analysis. *Glob Change Biol.* 26, 1638–1653.  
598 <http://dx.doi.org/10.1111/gcb.14933>

599 Tong, C., Morris, J.T., Huang, J.F., Xu, H., Wan, S.A., 2018. Changes in pore-water  
600 chemistry and methane emission following the invasion of *Spartina alterniflora* into  
601 an oligohaline marsh. *Limnol. Oceanogr.* 63, 384–396.  
602 <https://doi.org/10.1002/lno.10637>

603 Tong, C., Wang, W.Q., Huang, J.F., Gauci, V., Zhang, L.H., Zeng, C.S., 2012. Invasive  
604 alien plants increase CH<sub>4</sub> emissions from a subtropical tidal estuarine wetland.  
605 *Biogeochemistry* 111, 677–693. <https://doi.org/10.1007/s10533-012-9712-5>

606 Turner, J.C., Moorberg, C.J., Wong, A., Shea, K., Waldrop, M.P., Turetsky, M.R., Neumann,  
607 R.B., 2020. Getting to the root of plant-mediated methane emissions and oxidation in  
608 a Thermokarst Bog. *J. Geophys. Res.-Biogeo.* 125, e2020JG005825.  
609 <https://doi.org/10.1029/2020JG005825>

610 Verhoeven, J.T.A., Setter, T.L., 2010. Agricultural use of wetlands: Opportunities and  
611 limitations. *Ann. Bot.* 105, 155–163. <https://doi.org/10.1093/aob/mcp172>

612 Villa, J.A., Ju, Y., Stephen, T., Rey-Sanchez, C., Wrighton, K.C., Bohrer, G., 2020. Plant-  
613 mediated methane transport in emergent and floating-leaved species of a temperate  
614 freshwater mineral-soil wetland. *Limnol. Oceanogr.* 65, 1635–1650.  
615 <https://doi.org/10.1002/lno.11467>

616 Vizza, C., West, W.E., Jones, S.E., Hart, J.A., Lamberti, G.A., 2017. Regulators of coastal  
617 wetland methane production and responses to simulated global change. *Biogeosciences*  
618 14, 431–446. <https://doi.org/10.5194/bg-14-431-2017>

619 Xiang, J., Liu, D.Y., Ding, W.X., Yuan, J.J., Lin, Y.X., 2015. Invasion chronosequence of  
620 *Spartina alterniflora* on methane emission and organic carbon sequestration in a  
621 coastal salt marsh. *Atmos. Environ.* 112, 72–80.  
622 <http://dx.doi.org/10.1016/j.atmosenv.2015.04.035>

623 Xiao, Q.T., Zhang, M., Hu, Z.H., Gao, Y.Q., Hu, C., Liu, C., Liu, S.D., Zhang, Z., Zhao,

624 J.Y., Xiao, W., Lee, X., 2017. Spatial variations of methane emission in a large shallow  
625 eutrophic lake in subtropical climate. *J. Geophys. Res. Biogeosci.* 122(7), 1597–1614.  
626 <https://doi.org/10.1002/2017JG003805>

627 Wang, C., Sun, H.F., Zhang, X.X., Zhang, J.N., Zhou, S., 2021a. Contributions of  
628 photosynthate carbon to methane emissions from rice paddies cultivated using different  
629 organic amendment methods: Results from an in-situ <sup>13</sup>C-labelling study. *Geoderma*,  
630 402, 115190. <https://doi.org/10.1016/j.geoderma.2021.115190>

631 Wang, G.Q., Xia, X.H., Liu, S.D., Zhang, L., Zhang, S.B., Wang, J.F., Xi, N.N., Zhang,  
632 Q.R., 2021b. Intense methane ebullition from urban inland waters and its significant  
633 contribution to greenhouse gas emissions. *Water Res.* 189, 116654.  
634 <https://doi.org/10.1016/j.watres.2020.116654>

635 Wang, W., Liu, H., Li, Y.Q., Su, J.L., 2014. Development and management of land  
636 reclamation in China. *Ocean Coast. Manag.* 102, 415–425.  
637 <https://doi.org/10.1016/j.ocecoaman.2014.03.009>

638 Wanninkhof, R., 1992. Relationship between wind speed and gas exchange over the ocean.  
639 *J. Geophys. Res.* 97, 7373–7382. <https://doi.org/10.1029/92JC00188>

640 Wassmann, R., Neue, H.U., Bueno, C., Lantin, R.S., Alberto, M.C.R., Buendia, L.V.,  
641 Bronson, K., Papen, H., Rennenberg, H., 1998. [Methane production capacities of  
642 different rice soils derived from inherent and exogenous substrates.](#) *Plant Soil* 203,  
643 [227–237.](#)

644 Wells, N.S., Maher, D.T., Erler, D.V., Hipsey, M., Rosentreter, J.A., Eyre, B.D., 2018.  
645 Estuaries as sources and sinks of N<sub>2</sub>O across a land use gradient in subtropical Australia.  
646 *Global Biogeochem. Cycles* 32(5), 877–894. <https://doi.org/10.1029/2017gb005826>

647 Wu, S., Li, S.Q., Zou, Z.H., Hu, T., Hu, Z.Q., Liu, S.W., Zou, J.W., 2019. High methane  
648 emissions largely attributed to ebullitive fluxes from a subtropical river draining a rice  
649 paddy watershed in China. *Environ. Sci. Technol.* 53, 349–3507.  
650 <https://doi.org/10.1021/acs.est.8b05286>

651 Yang, B., Li, X.Z., Lin, S.W., Jiang, C., Xue, L.M., Wang, J.J., Liu, X.T., Espenberg, M.,

652 Pärn, J., Mander, Ü., 2021. Invasive *Spartina alterniflora* changes the Yangtze Estuary  
653 salt marsh from CH<sub>4</sub> sink to source. *Estuar. Coast. Shelf S.* 252, 107258.  
654 <https://doi.org/10.1016/j.ecss.2021.107258>

655 Yang, P., Bastviken, D., Jin, B.S., Mou, X.J., Tong, C., 2017. Effects of coastal marsh  
656 conversion to shrimp aquaculture ponds on CH<sub>4</sub> and N<sub>2</sub>O emissions. *Estuar. Coast.*  
657 *Shelf S.* 199, 125–131. <https://doi.org/10.1016/j.ecss.2017.09.023>

658 Yang, P., Tang, K.W., Tong, C., Lai, D.Y.F., Wu, L.Z., Yang, H., Zhang, L.H., Tang, C.,  
659 Hong, Y., Zhao, G.H., 2022. Changes in sediment methanogenic archaea community  
660 structure and methane production potential following conversion of coastal marsh to  
661 aquaculture ponds. *Environ. Pollut.* 305, 119276.  
662 <https://doi.org/10.1016/j.envpol.2022.119276>

663 Yang, P., Zhang, Y., Yang, H., Zhang, Y.F., Xu, J., Tan, L.S., Tong, C., Lai, D.Y.F., 2019a.  
664 Large fine-scale spatiotemporal variations of CH<sub>4</sub> diffusive fluxes from shrimp  
665 aquaculture ponds affected by organic matter supply and aeration in Southeast China.  
666 *J. Geophys. Res.-Biogeo.* 124, 1290–1307. <https://doi.org/10.1029/2019JG005025>

667 Yang, P., Lai, D.Y.F., Yang, H., Tong, C., Lebel, L., Huang, J., Xu, J., 2019b. Methane  
668 dynamics of aquaculture shrimp ponds in two subtropical estuaries, southeast China:  
669 Dissolved concentration, net sediment release, and water oxidation. *J. Geophys. Res.-*  
670 *Biogeo.* 124, 1430–1445. <https://doi.org/10.1029/2018JG004794>

671 Yang, P., Zhang, Y.F., Yang, H., Guo, Q.Q., Lai, D.Y.F., Zhao, G.H., Li, L., Tong, C., 2020.  
672 Ebullition was a major pathway of methane emissions from the aquaculture ponds in  
673 southeast China. *Water Res.* 184, 116176.  
674 <https://doi.org/10.1016/j.watres.2020.116176>

675 Yuan, J.J., Liu, D.Y., Xiang, J., He, T.H., Kang, H., Ding, W.X., 2021. Methane and nitrous  
676 oxide have separated production zones and distinct emission pathways in freshwater  
677 aquaculture ponds. *Water Res.* 190, 116739.  
678 <https://doi.org/10.1016/j.watres.2020.116739>

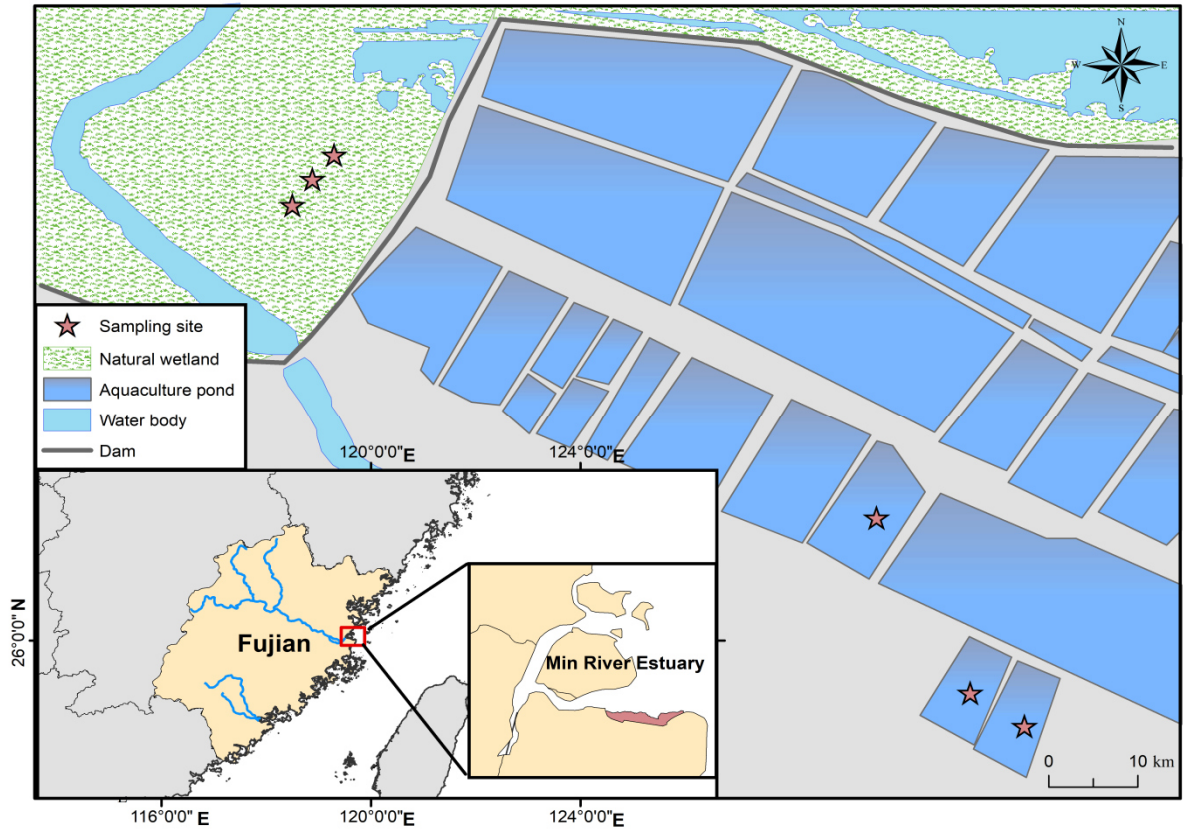
679 Zhang, L.W., Xia, X.H., Liu, S.D., Zhang, S.B., Li, S.L., Wang, J.F., Wang, G.Q., Gao, H.,

680 Zhang, Z.R., Wang, Q.R., Wen, W., Liu, R., Yang, Z.F., Stanley, E.H., Raymond, P.A.,  
681 2020. Significant methane ebullition from alpine permafrost rivers on the East  
682 Qinghai–Tibet Plateau. *Nat. Geosci.* 13, 349–354. [https://doi.org/10.1038/s41561-020-](https://doi.org/10.1038/s41561-020-0571-8)  
683 [0571-8](https://doi.org/10.1038/s41561-020-0571-8)

684 Zhou, C.Q., Peng, Y., Yu, M.T., Deng, Y., Chen, L., Zhang, L.Q., Xu, X.G., Zhang, S.Y., Y,  
685 Yan., Wang, G.X., 2022. Severe cyanobacteria accumulation potentially induces  
686 methylotrophic methane producing pathway in eutrophic lakes. *Environ. Pollut.*  
687 292(Part B), 118443. <https://doi.org/10.1016/j.envpol.2021.118443>

**Table 1**  
 Summary of two-way ANOVAs examining the effect of habitat types (*HT*), sampling season (*SS*) and their interactions on sediment and porewater properties.

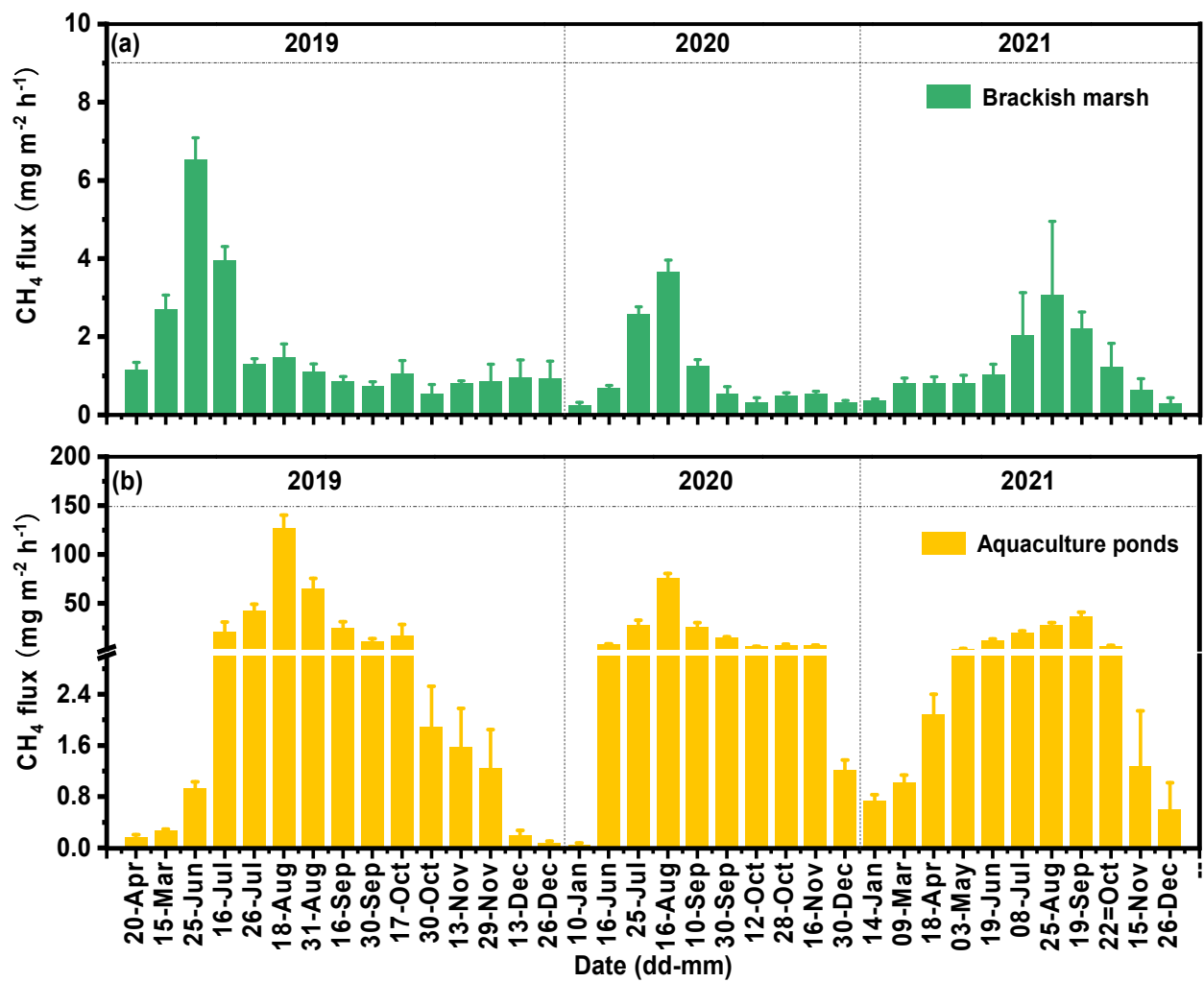
<i>df</i>	Sediment properties				Porewater properties										
	Temperature ( <i>T</i> s)		Salinity		Total carbon (TC)		Total nitrogen (TC)		NH <sub>4</sub> <sup>+</sup> -N		Cl <sup>-</sup>		SO <sub>4</sub> <sup>2-</sup>		
	<i>F</i> values	<i>P</i> values	<i>F</i> values	<i>P</i> values	<i>F</i> values	<i>P</i> values	<i>F</i> values	<i>P</i> values	<i>F</i> values	<i>P</i> values	<i>F</i> values	<i>P</i> values	<i>F</i> values	<i>P</i> values	
<b><i>HT</i></b>	<b>1</b>	70.663	<0.001	41.227	<0.001	2.322	=0.043	51.253	<0.001	20.102	<0.001	14.847	<0.001	0.245	0.622
<b><i>SS</i></b>	<b>3</b>	74.999	<0.001	14.611	<0.001	12.755	<0.001	2.489	=0.001	2.145	=0.106	13.108	<0.001	15.660	<0.001
<b><i>HT</i>×<i>SS</i></b>	<b>3</b>	5.194	=0.003	12.394	<0.001	2.289	=0.089	6.679	=0.001	26.583	<0.001	7.376	<0.001	6.265	=0.001



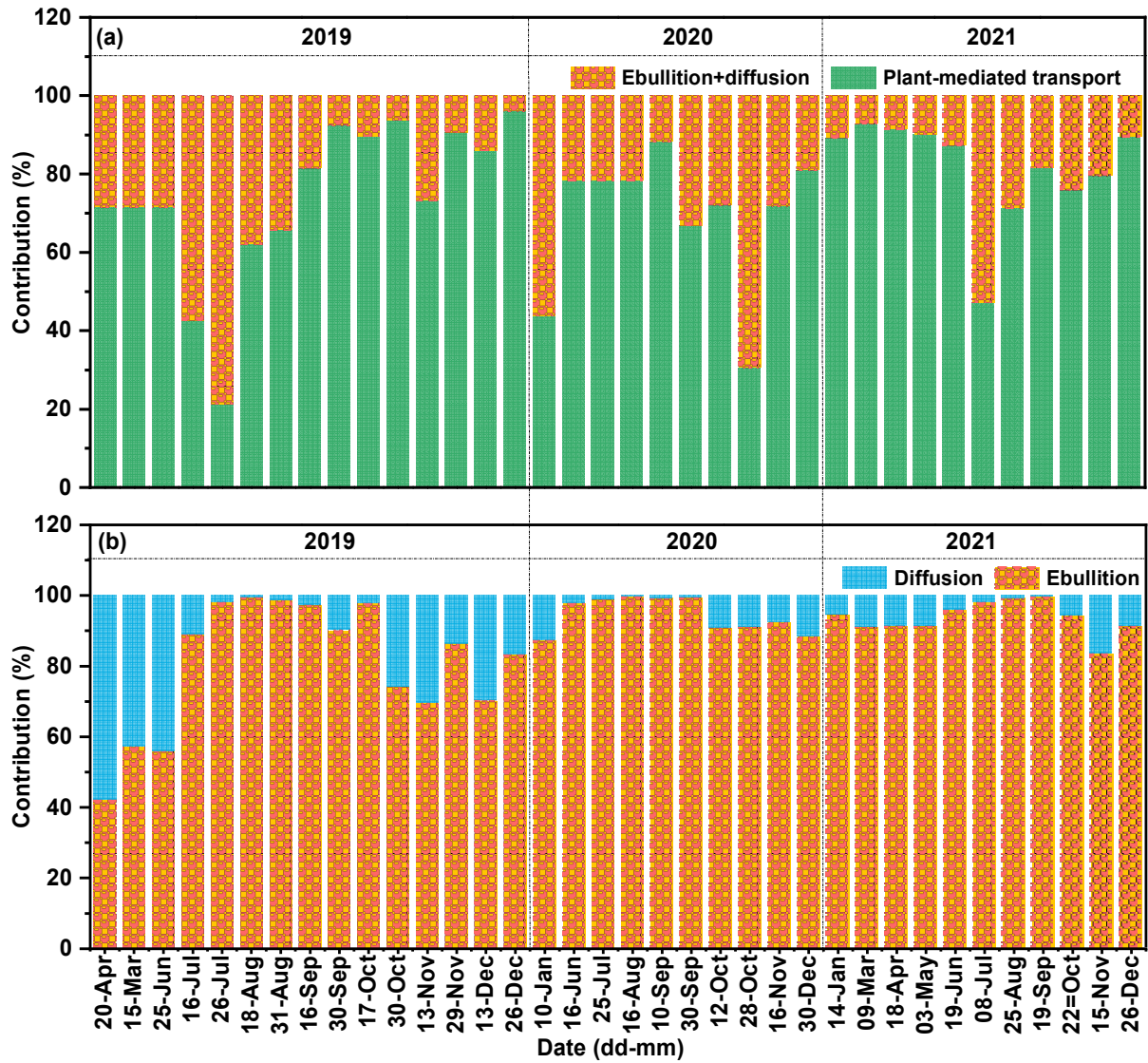
1

2 **Figure 1.** Location of sampling sites in a *Cyperus malaccensis* marsh and nearby  
3 aquaculture ponds in the Shanyutan Wetland, southeastern China.



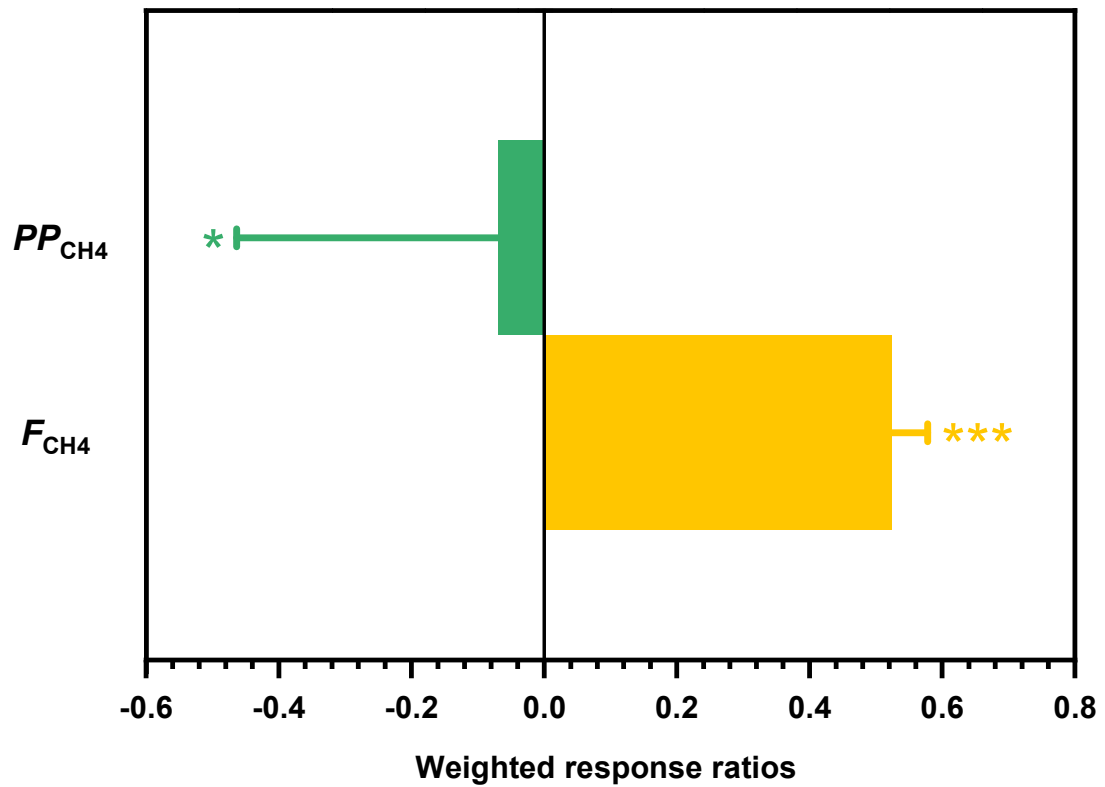


4  
5 **Figure 2.** Temporal data of CH<sub>4</sub> emission flux in the marsh and aquaculture ponds. Bars represent  
6 mean ± SE (*n* = 3).



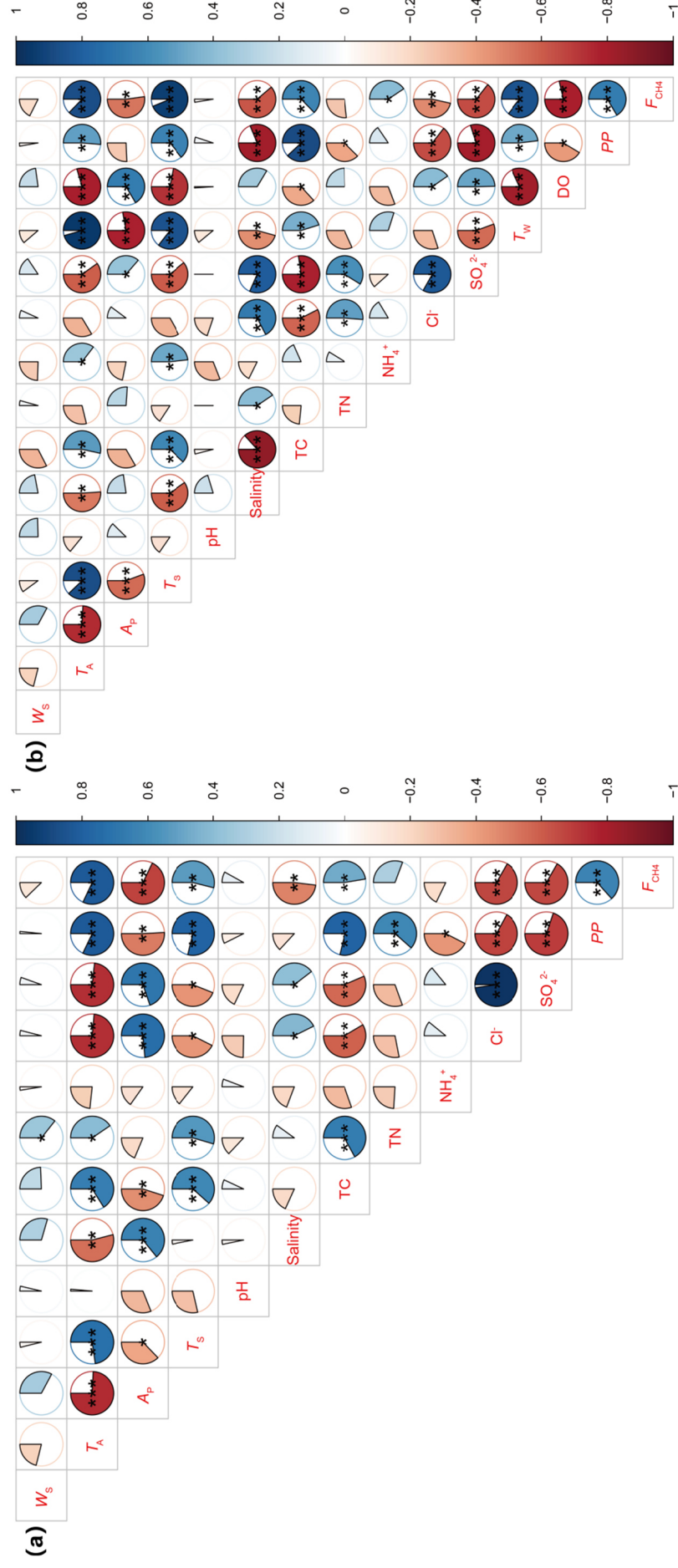
7

8 **Figure 3.** Temporal data of contributions of different transport pathways to CH<sub>4</sub> emission in (a)  
 9 the marsh and (b) the aquaculture ponds.



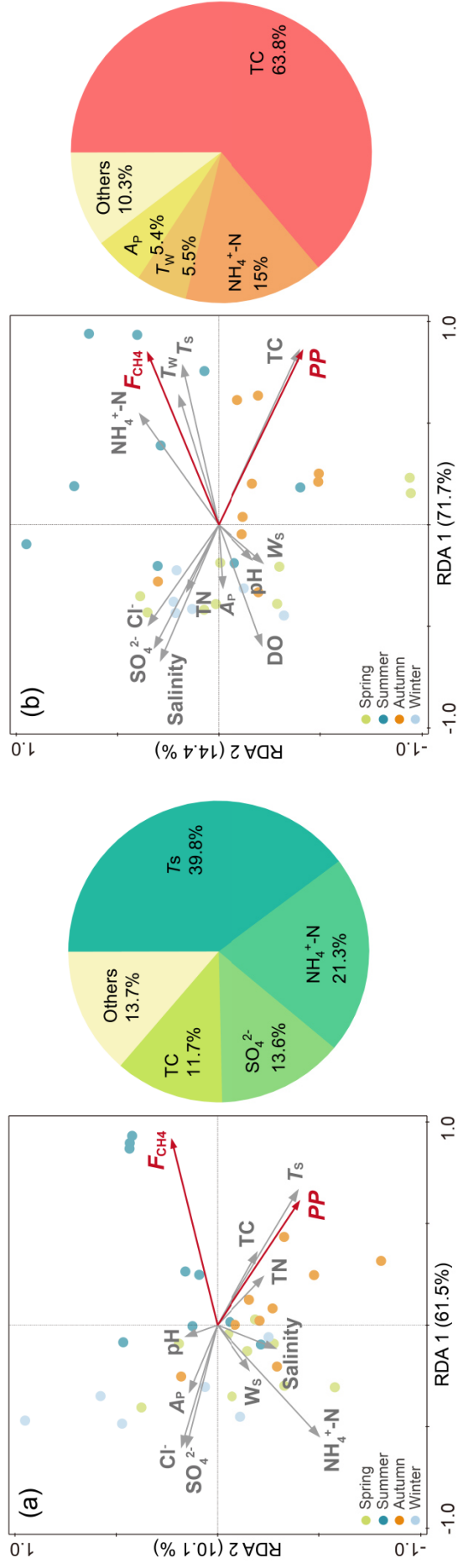
10

11 **Figure 4.** Weighted response ratios (RR<sub>++</sub>) of (a) sediment CH<sub>4</sub> production potential  
 12 ( $PP_{CH_4}$ ) and (b) CH<sub>4</sub> emission flux ( $F_{CH_4}$ ) for the conversion of brackish marsh to  
 13 aquaculture ponds. Bars represent the RR<sub>++</sub> values and 95% CIs ( $n = 63$ ). Effect of  
 14 habitat modification was significant for both parameters (\*  $p < 0.05$ ; \*\*\*  $p < 0.001$ ).



15

16 **Figure 5.** Correlation matrix for (a) the brackish marsh, and (b) the aquaculture ponds. Colors of the circle segments indicate the direction of  
 17 correlation (blue = positive; red = negative); size of the colored segment is proportional to the  $r$  value (between -1 and 1). Asterisks within each  
 18 circle indicate level of significance (\* $p < 0.05$ ; \*\* $p < 0.01$ ; \*\*\* $p < 0.001$ ).  $W_s$ ,  $T_A$ ,  $A_p$ ,  $T_s$ , TC, TN,  $T_w$ , DO, PP and  $F_{CH_4}$  represent wind speed,  
 19 air temperature, atmospheric pressure, sediment temperature, total carbon, total nitrogen, water temperature, dissolved oxygen, CH<sub>4</sub> production  
 20 potential and CH<sub>4</sub> emission flux, respectively.



21

22 **Figure 6.** Results of redundancy analysis (RDA) between  $CH_4$  emission flux ( $F_{CH4}$ ) [or sediment  $CH_4$  production potential ( $PP$ )] and

23 environmental variables in (a) the marsh, and (b) the aquaculture ponds, showing the loadings of the different environmental variables.  $W_s$ ,  $AP$ ,  $T_s$ ,

24  $TC$ ,  $TN$ ,  $T_w$  and  $DO$  represent wind speed, atmospheric pressure, sediment temperature, total carbon, total nitrogen, water temperature and

25 dissolved oxygen, respectively. The pie charts show the percentages of the variance of  $F_{CH4}$  explained by the different variables.

1 **Supporting Information**

2 **Large increase in CH<sub>4</sub> emission following conversion of coastal**  
3 **marsh to aquaculture ponds explained by gas transport pathways**

4 Ping Yang<sup>a,b</sup>, Derrick Y.F. Lai<sup>c</sup>, Hong Yang<sup>d,e</sup>, Yongxin Lin<sup>a,b</sup>, Chuan Tong<sup>a,b\*</sup>, Yan Hong<sup>b</sup>,  
5 Yalan Tian<sup>b</sup>, Chen Tang<sup>b</sup>, Kam W. Tang<sup>f\*</sup>

6 <sup>a</sup>*Key Laboratory of Humid Subtropical Eco-geographical Process of Ministry of Education, Fujian*  
7 *Normal University, Fuzhou 350007, P.R. China*

8 <sup>b</sup>*School of Geographical Sciences, Fujian Normal University, Fuzhou 350007, P.R. China*

9 <sup>c</sup>*Department of Geography and Resource Management, The Chinese University of Hong Kong, Hong*  
10 *Kong, China*

11 <sup>d</sup>*College of Environmental Science and Engineering, Fujian Normal University, Fuzhou 350007,*  
12 *P.R. China*

13 <sup>e</sup>*Department of Geography and Environmental Science, University of Reading, Reading, RG6 6AB, UK*

14 <sup>f</sup>*Department of Biosciences, Swansea University, Swansea SA2 8PP, U. K.*

15

16

17

18 **\*Correspondence to:**

19 tongch@fjnu.edu.cn (Chuan Tong); k.w.tang@swansea.ac.uk (Kam W. Tang)

20 **Supporting Information Summary**

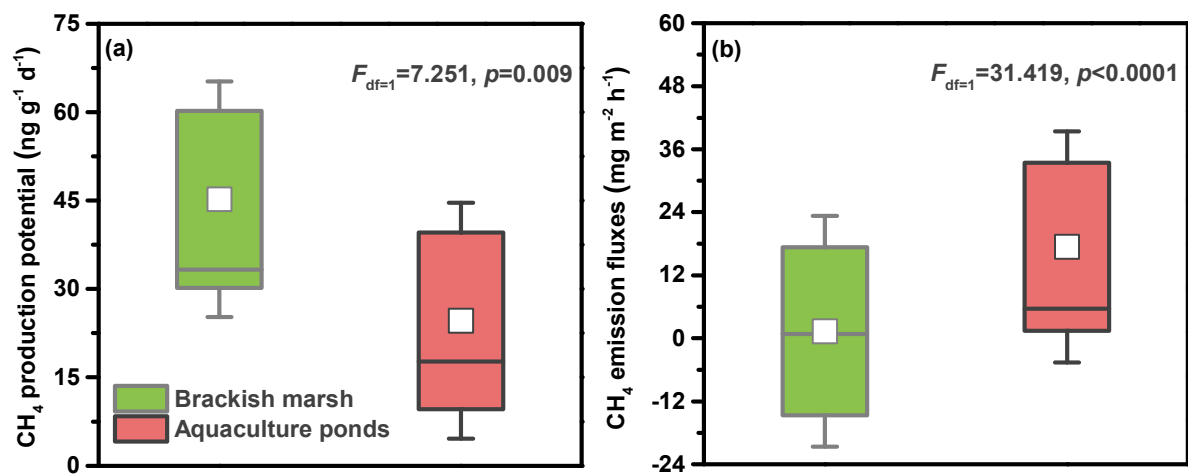
21 **No. of pages: 7**      **No. of figures: 2**      **No. of tables: 2**

22 **Page S3:** Figure S1. Boxplots of (a) sediment CH<sub>4</sub> production potential ( $n = 60$ ) and (b)  
23 CH<sub>4</sub> emission flux ( $n = 216$ ) in the brackish marsh and aquaculture ponds.

24 **Page S4:** Figure S2. Boxplots of seasonal CH<sub>4</sub> emission flux in (a) the brackish marsh,  
25 and (b) the aquaculture ponds. Different lowercase letters within each panel indicate  
26 significant differences at the  $p < 0.05$  level between the seasons.

27 **Page S5:** Table S1 Physicochemical properties of the sediment and porewater in the  
28 brackish marsh and aquaculture ponds. Different lowercase letters within the same row  
29 indicate significant differences at  $p < 0.05$  level between the two habitats.

30 **Page S6:** Table S2 Linear relationship between CH<sub>4</sub> emission flux ( $F_{\text{CH}_4}$ ,  $\text{mg m}^{-2} \text{h}^{-1}$ ) and  
31 sediment salinity ( $Sal_{\text{sed}}$ , ‰) in the brackish marsh and aquaculture ponds.

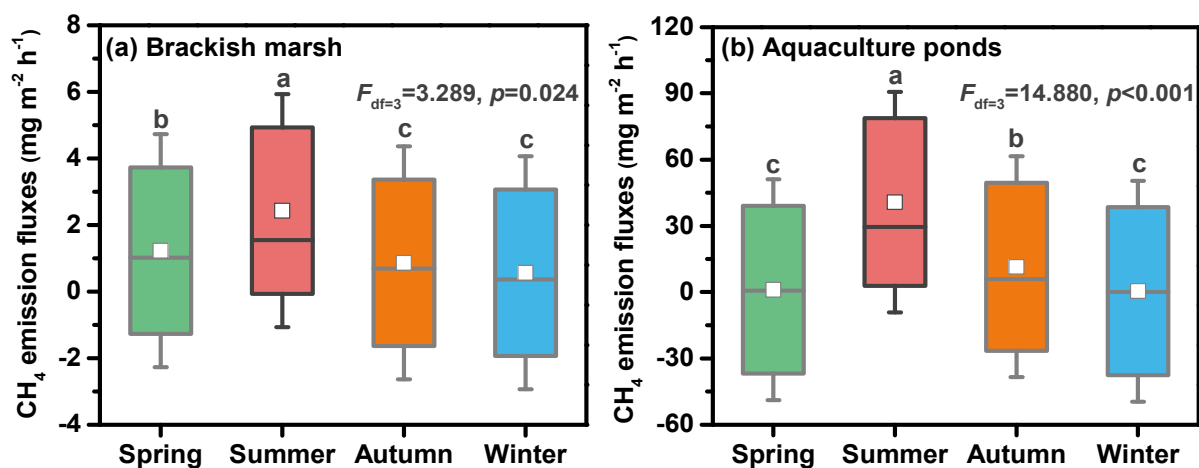


32

33 **Figure S1.** Boxplots of (a) sediment CH<sub>4</sub> production potential ( $n = 60$ ) and (b) CH<sub>4</sub> emission

34 flux ( $n = 216$ ) in the brackish marsh and aquaculture ponds.





35

36 **Figure S2.** Boxplots of seasonal CH<sub>4</sub> emission flux in (a) the brackish marsh, and (b) the  
 37 aquaculture ponds. Different lowercase letters within each panel indicate significant  
 38 differences at the  $p < 0.05$  level between seasons.

39 **Table S1**

40 Physicochemical properties of sediment and porewater in the brackish marsh and aquaculture ponds (mean±SE). Different lowercase letters within  
 41 the same row indicate significant differences at  $p < 0.05$  level between the two habitats.

Environmental variables	Brackish marsh					Aquaculture ponds				
	Spring	Summer	Autumn	Winter	Mean	Spring	Summer	Autumn	Winter	Mean
<b>Sediment</b>										
Temperature (°C)	23.6±0.3	28.2±0.1	27.8±0.6	17.6±1.2	24.7±0.8a	18.5±0.7	24.6±1.2	21.5±2.6	16.4±0.8	20.4±0.6b
pH	6.7±0.1	7.0±0.4	6.6±0.1	6.6±0.1	6.7±0.1a	6.8±0.3	6.7±0.1	6.9±0.1	6.7±0.1	6.7±0.1a
Salinity (‰)	2.6±0.1	2.8±0.3	7.8±0.5	10.8±0.4	6.0±1.9a	2.7±0.4	2.2±0.2	2.2±0.2	3.25±0.4	2.5±0.2b
TC (g kg <sup>-1</sup> )	13.1±2.9	27.8±2.2	22.2±1.4	10.6±2.9	18.4±3.9a	15.7±3.4	18.6±2.3	19.6±2.1	9.6±1.4	15.9±2.3b
TN (g kg <sup>-1</sup> )	1.3±0.1	1.9±0.2	1.0±0.1	0.7±0.3	1.3±0.1a	0.6±0.1	0.7±0.1	0.7±0.1	0.5±0.2	0.7±0.1b
<b>Porewater</b>										
NH <sub>4</sub> <sup>+</sup> -N (mg L <sup>-1</sup> )	0.9±0.1	0.3±0.1	0.5±0.1	0.4±0.1	0.5±0.1a	0.1±0.1	0.2±0.1	0.3±0.1	0.4±0.1	0.3±0.1b
NO <sub>3</sub> <sup>-</sup> -N (mg L <sup>-1</sup> )	0.9±0.1	0.5±0.1	0.3±0.1	0.3±0.1	0.5±0.1a	0.1±0.1	0.4±0.1	0.1±0.1	0.2±0.1	0.2±0.1b
Cl <sup>-</sup> (mg L <sup>-1</sup> )	5405±2528	135±29	6639±620	9090±932	5317±1889a	2090±671	2406±1470	1967±483	4803±858	2816±668b
SO <sub>4</sub> <sup>2-</sup> (mg L <sup>-1</sup> )	874±393	48±9	1099±90	1462±136	871±299a	664±150	678±133	581±168	1347±154	817±177a
<b>Surface water</b>										
Temperature (°C)	ND	ND	ND	ND	ND	22.9±0.6	29.9±0.3	23.2±0.8	13.8±0.8	22.4±3.3
DO (mg L <sup>-1</sup> )	ND	ND	ND	ND	ND	8.6±0.4	5.4±0.2	7.9±1.1	11.2±0.3	8.3±1.2

42 TC, Total carbon; TN, Total nitrogen; DO, Dissolved oxygen; ND, No data. Data are after Yang *et al.* [2022] for reference and review only.

43 **Table S2**

44 Linear relationship between CH<sub>4</sub> emission flux ( $F_{\text{CH}_4}$ , mg m<sup>-2</sup> h<sup>-1</sup>) and sediment salinity ( $Sal_{\text{sed}}$ , ‰) in the brackish marsh and aquaculture  
 45 ponds.

Habitat type	Linear regression equation	$r^2$	$p$ value	$n$
Brackish marsh	$F_{\text{CH}_4} = -0.3635Sal_{\text{sed}} + 3.7389$	0.53	<0.01	9
Aquaculture ponds	$F_{\text{CH}_4} = -2.5831Sal_{\text{sed}} + 29.391$	0.43	<0.01	9

46

47 **Reference**

48 Yang, P., Tang, K. W., Tong, C., Lai, D. Y. F., Wu, L. Z., Yang, H., Zhang, L. H., Tang,  
49 C., Hong, Y., Zhao, G. H., 2022. Changes in sediment methanogenic archaea  
50 community structure and methane production potential following conversion of  
51 coastal marsh to aquaculture ponds. *Environm. Pollut.* 305, 119276.  
52 <https://doi.org/10.1016/j.envpol.2022.119276>